Advances in Military Technology
Vol. 17, No. 2, 2022, pp. 357-382
ISSN 1802-2308, eISSN 2533-4123
DOI 10.3849/aimt.01498

Hybrid Positioning Technique Based Integration of GPS/INS for an Autonomous Vehicle Navigation

A. N. Ouda and A. Mohamed*

Faculty of Engineering and Applied Science,
University of Ontario Institute of Technology (UOIT), Canada

The manuscript was received on 4 April 2021 and was accepted after revision for publication as research paper on 24 October 2022.

Abstract:

This paper presents a hybrid positioning technique combining both loosely and tightly coupled Kalman Filter (KF) algorithms for an autonomous multi-wheeled combat vehicle. The developed algorithm is able to provide accurate positioning information even if number of visible satellites falls below the minimum due to the harsh operation environments. Two modes of operation were considered which automatically switch between them according to the number of visible satellites in order to correct the INS drift. Furthermore, a performance comparison between fifteen and eighteen KFs states is conducted. A simulation of the developed algorithm is performed, using a SATNAV navigation toolbox and the collected data from real sensors mounted on a ground vehicle. The experimental results validated effectiveness of the developed algorithm.

Keywords:

autonomous vehicles, GPS/INS navigation systems, hybrid positioning technique, Kalman filter, sensor fusion

1 Introduction

In the last few years, the autonomous vehicles have become increasingly important assets in various civilian and military operations. Such vehicles have the capabilities to work and react to its environment autonomously [1-3]. Consequently, building autonomous combat vehicles has drawn dramatic attention while autonomous road vehicles are the boosting research topics [4, 5].

The most widely used navigation sensors for autonomous vehicles are GPS and INS. Such sensors can be used individually or integrated [6-8]. In addition, using an Inertial Measurement Units (IMU) in autonomous vehicles, the acceleration, angular rotation, and attitude data are provided at high update rates. Accordingly, the velocity and position of the vehicle can be estimated easily. Furthermore, IMU sensors are not

* *Corresponding author: Faculty of Engineering and Applied Science, University of Ontario Institute of Technology (UOIT), 2000 Simcoe St N, Oshawa, ON L1G0C5, Canada. E-mail: Amr.Mohamed@uoit.net. ORCID 0000-0002-2185-6153.*

affected by the vehicle's tires slip that is encountered by most ground vehicle applications. On the other hand, GPS receiver is an absolute low-frequency sensor that provides the state information at low updated rates. Consequently, the integration of these two sensors will improve the position information for the autonomous vehicle during a maneuver.

The combination of data from several sensors is known as sensors fusion. This combination, or integration, enhances the accuracy, which is not realizable when employing each sensor individually. The main purpose of applying data fusion is to eliminate the possibility of detectable errors and to obtain a higher rate of reliability by using data from several distributed sensors. On the other hand, Kalman Filter (KF) is the most popular approach in integrated navigation systems which considers a powerful mathematical tool for analyzing and solving localization estimation problems [9-13]. KF was originally introduced by Kalman [14], and has been extensively applied especially in navigation applications, which were implemented to fuse low-level data. Furthermore, Extended KF (EKF) is one of the most readily employed methods for fusing data in case of applications utilizing robots.

An EKF has proved to be a promising approach to fuse INS and GPS [15], which obtains high accuracy and stable positioning solution with two-antenna GPS/INS integration in harsh environments using the conventional EKF GPS/INS integration. In addition, it provides monitoring the contribution of the filter dynamic model by adaptive modification of noise covariance. The accuracy of the introduced technique has been verified with a field vehicular test. [16], proposed a standalone attitude and heading reference system (AHRS) methodology that employs the IMU and magnetometers data in an averaging manner. This method takes the rotations of the platform into account. The introduced AHRS has the capability to provide attitude updates through a refined loosely coupled filtering procedure. A GPS/IMU sensor fusion system using KF estimation methods using fuzzy subsets was discussed by Caron [17], for autonomous ground vehicles. Due to the possible loss of the GPS signal and as a result of the INS drift, the multi-sensor KF could be fed directly via the acceleration obtained from IMU.

Lee [18] introduced a sensor fusion algorithm, which fuses the obtained data from both the monocular camera and GPS/IMU for autonomous system. Accordingly, it enhances the accuracy and robustness of the navigation system. Wang [19] introduced an accurate GPS/IMU/dead reckoning system fusion algorithm for unmanned ground vehicles, which is based on autoregressive moving average models and occupancy grid constraints. In addition, a GPS/IMU sensor fusion system using KF estimation methods using fuzzy subsets was discussed by Bostanci [20] for autonomous ground vehicles. Due to the possible loss of the GPS signal and as a result of the INS drift, the multi-sensor KF could be fed directly via the acceleration obtained from IMU. Tian [21] introduced a variational Bayesian Kalman Filter (VBKF) algorithm for INS/GPS integrated in order to overcome the performance degradation which comes from the outliers in the traditional filtering.

In this paper, a hybrid framework for positioning technique based on the integration of GPS/INS for combat vehicles is developed. The proposed framework will solve the positioning accuracy problem when the number of visible satellites is less than four. The proposed algorithm has the capability to adapt itself to solving the positioning problem by switching between the loosely coupled and tightly coupled algorithms according to the number of visible satellites. Two KFs are developed; the first is to improve GPS information, and the second enhances the INS position, velocity, and the

attitude with the aid of GPS position and velocity. The advantage of the developed methodology is that it is based on low cost sensors and the proposed algorithm able to provide accurate and reliable navigation guidance.

The paper is structured as follows. The methodology of the proposed hybrid positioning technique is presented in section 2. Section 3 introduces the construction of Kalman filter for the proposed hybrid technique. The numerical simulation and field test for the proposed hybrid positioning technique are presented in Section 4. The conclusion is given in Section 5.

2 GPS/INS Hybrid Positioning Technique

In this section, the methodology of the proposed hybrid positioning technique is described. In order to achieve accurate and robust positioning estimation for the autonomous multi-wheeled combat vehicle, a hybrid positioning technique based on a KF method is proposed. The developed technique fuses the data from the low-cost GPS and INS sensors. In addition, it contains two modes of operation, which provide an accurate navigation solution during maneuvers by updating the mode according to the GPS signal and the availability of the satellites.

If the GPS signal is available, and the number of visible satellites is sufficient, the developed framework will be operated in the first mode based on loosely coupled Kalman filter GPS/INS integration as shown in Fig. 1a. Consequently, the GPS and INS will operate independently to provide two independent navigation solutions. Therefore, to get the third navigation solution, the obtained data from the GPS and INS will be fed to Kalman filter (fused together). By taking the difference between the collected data and based on the error models, the INS errors can be estimated. Based on the estimated errors, the INS solution will be corrected and consequently provide the integrated navigation solution. The main feature of loosely coupled KF is that two separate KF of the GPS and the integration filter are used in cascaded integration.

On the other hand, when GPS signal lacks credibility or the effective number of satellites less than four, the developed framework will switch to the second mode that is based on tightly coupled KF as shown in Fig. 1b. Both GPS and INS work as basic sensors providing their raw outputs of pseudorange and pseudorange rate measurements. The difference between the pseudorange and pseudorange rate measurements from the GPS and the INS are processed directly in the navigation KF to estimate the INS errors. According to the estimated errors, the INS output can be corrected, and the integrated navigation solution can be obtained. By this way, aiding the INS with the raw GPS measurements is possible even if the number of visible satellites is below the minimum [22, 23]. Therefore, the use of the proposed hybrid algorithm has benefits for combat vehicle navigation system when the satellite signals are difficult to receive.

3 Construction of Kalman Filtering Algorithm

In this section, the construction of Kalman filter for the proposed hybrid technique is described.

3.1 Enhance GPS Using Kalman Filter

The purpose of KF is to improve and enhance the GPS data before fusing it with INS data. The continuous-time system state equation of KF can be expressed as

$$\dot{\boldsymbol{X}}(t)=\boldsymbol{F}(t)\boldsymbol{X}(t)+\boldsymbol{G}(t)\boldsymbol{W}(t) \tag{1}$$

where
$\boldsymbol{F}(t)$ is called the dynamic matrix, which propagates the errors over time,
$\boldsymbol{X}(t)$ is the state vector,
$\boldsymbol{G}(t)$ is the noise distribution matrix,
$\boldsymbol{W}(t)$ is the random forcing functions.

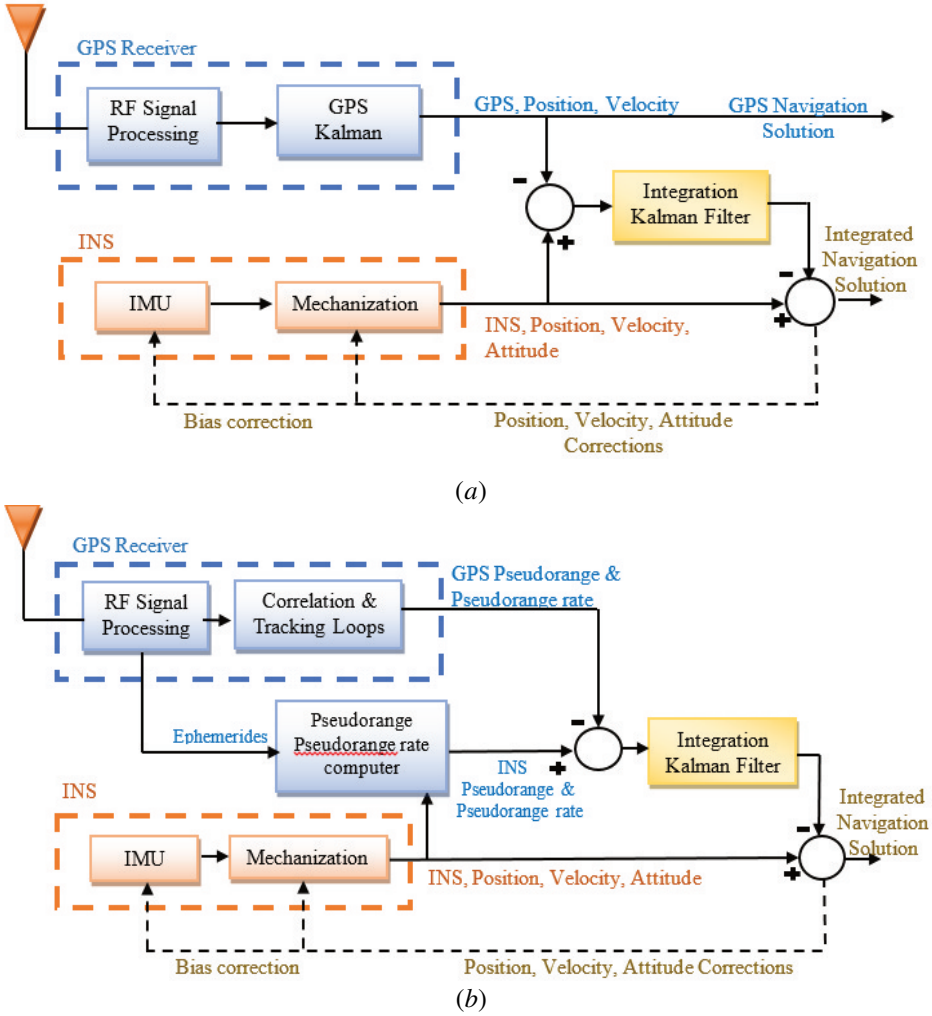

Fig. 1 Proposed hybrid positioning methodology. (a) The first mode loosely coupled KF; (b) The second mode tightly coupled KF

Consequently, based on the discretizing method in [24], the discrete time linear system, can be expressed as follows:

$$\boldsymbol{X}_k=\boldsymbol{\varphi}_{k,k-1}\boldsymbol{X}_{k-1}+\boldsymbol{G}_{k-1}\boldsymbol{W}_{k-1} \tag{2}$$

where
$\boldsymbol{x}_k$ is the state vector,
$\boldsymbol{\varphi}_{k,k-1}$ is the state transition matrix,
$\boldsymbol{G}_{k-1}$ is the noise distribution matrix,
$\boldsymbol{W}_{k-1}$ is the process noise vector, k is the measurement epoch.

Then, the state vector $\boldsymbol{X}$ will be defined as follows:

$$\boldsymbol{X} = \begin{bmatrix} \delta_{\mathrm{N}} & \delta_{\mathrm{E}} & \delta_{\mathrm{U}} & \delta_{\mathrm{VN}} & \delta_{\mathrm{VE}} & \delta_{\mathrm{VU}} & \delta_{\mathrm{Offset}} & \delta_{\mathrm{drift}} \end{bmatrix}^{\mathrm{T}} \tag{3}$$

where
$\begin{bmatrix} \delta_{\mathrm{N}} & \delta_{\mathrm{E}} & \delta_{\mathrm{U}} \end{bmatrix}$ denote the north, east and up positions respectively,
$\begin{bmatrix} \delta_{\mathrm{VN}} & \delta_{\mathrm{VE}} & \delta_{\mathrm{VU}} \end{bmatrix}$ denote the north, east and up velocities respectively,
$\begin{bmatrix} \delta_{\mathrm{Offset}} & \delta_{\mathrm{drift}} \end{bmatrix}$ are the receiver clock offset and drift.

The initial state vector prediction is presented in Eq. (4), and the initial prediction error covariance matrix in Eq. (5)

$$\hat{\boldsymbol{X}}_0 = \begin{bmatrix} 0 & 0 & 0 & 0 & 0 & 0 & 0 & 0 & 0 \end{bmatrix}^{\mathrm{T}} \tag{4}$$

$$\boldsymbol{P}_0 = \begin{bmatrix} 10 & \cdots & 0 \\ \vdots & \ddots & \vdots \\ 0 & \cdots & 10 \end{bmatrix} \tag{5}$$

Considering Eq. (1), the dynamic matrix will be considered as shown in Eq. (6) and the overall system will be represented as follows:

$$\boldsymbol{F} = \begin{bmatrix} 0 & 0 & 0 & 1 & 0 & 0 & 0 & 0 \\ 0 & 0 & 0 & 0 & 1 & 0 & 0 & 0 \\ 0 & 0 & 0 & 0 & 0 & 1 & 0 & 0 \\ 0 & 0 & 0 & 1 & 0 & 0 & 0 & 0 \\ 0 & 0 & 0 & 0 & 1 & 0 & 0 & 0 \\ 0 & 0 & 0 & 0 & 0 & 1 & 0 & 0 \\ 0 & 0 & 0 & 0 & 0 & 0 & 0 & 0 \\ 0 & 0 & 0 & 0 & 0 & 0 & 0 & 0 \end{bmatrix} \tag{6}$$

$$\begin{bmatrix} \dot{\delta}_{\mathrm{N}} \\ \dot{\delta}_{\mathrm{E}} \\ \dot{\delta}_{\mathrm{U}} \\ \dot{\delta}_{\mathrm{VN}} \\ \dot{\delta}_{\mathrm{VE}} \\ \dot{\delta}_{\mathrm{VU}} \\ \dot{\delta}_{\mathrm{Offset}} \\ \dot{\delta}_{\mathrm{drift}} \end{bmatrix} = \begin{bmatrix} 0 & 0 & 0 & 1 & 0 & 0 & 0 & 0 \\ 0 & 0 & 0 & 0 & 1 & 0 & 0 & 0 \\ 0 & 0 & 0 & 0 & 0 & 1 & 0 & 0 \\ 0 & 0 & 0 & 1 & 0 & 0 & 0 & 0 \\ 0 & 0 & 0 & 0 & 1 & 0 & 0 & 0 \\ 0 & 0 & 0 & 0 & 0 & 1 & 0 & 0 \\ 0 & 0 & 0 & 0 & 0 & 0 & 0 & 0 \\ 0 & 0 & 0 & 0 & 0 & 0 & 0 & 0 \end{bmatrix} \begin{bmatrix} \delta_{\mathrm{N}} \\ \delta_{\mathrm{E}} \\ \delta_{\mathrm{U}} \\ \delta_{\mathrm{VN}} \\ \delta_{\mathrm{VE}} \\ \delta_{\mathrm{VU}} \\ \delta_{\mathrm{Offset}} \\ \delta_{\mathrm{drift}} \end{bmatrix} + \begin{bmatrix} 1 & 0 & 0 & 1 & 0 & 0 & 0 & 0 \\ 0 & 1 & 0 & 0 & 1 & 0 & 0 & 0 \\ 0 & 0 & 1 & 0 & 0 & 1 & 0 & 0 \\ 0 & 0 & 0 & 1 & 0 & 0 & 0 & 0 \\ 0 & 0 & 0 & 0 & 1 & 0 & 0 & 0 \\ 0 & 0 & 0 & 0 & 0 & 1 & 0 & 0 \\ 0 & 0 & 0 & 0 & 0 & 0 & 1 & 0 \\ 0 & 0 & 0 & 0 & 0 & 0 & 0 & 1 \end{bmatrix} \begin{bmatrix} W_{\mathrm{N}} \\ W_{\mathrm{E}} \\ W_{\mathrm{U}} \\ W_{\mathrm{VN}} \\ W_{\mathrm{VE}} \\ W_{\mathrm{VU}} \\ W_{\mathrm{Offset}} \\ W_{\mathrm{drift}} \end{bmatrix} \tag{7}$$

The state transition matrix Eq. (8) represents the known dynamic behavior of the system, which relates the state vector from epoch $k-1$ to epoch k.

$$\boldsymbol{\varphi} = \mathrm{e}^{\boldsymbol{F}\Delta t} \cong \boldsymbol{I} + \boldsymbol{F}\Delta t \tag{8}$$

where $\boldsymbol{I}$ is the identity matrix, Δt is the sampling interval.

Consequently, the discrete-time of the power spectral density can be expressed as follows:

$$\boldsymbol{Q}_k = \int_0^{\Delta t} \boldsymbol{\varphi} \boldsymbol{G} \boldsymbol{Q} \boldsymbol{G}^{\mathrm{T}} \boldsymbol{\varphi}^{\mathrm{T}} \mathrm{d}t \tag{9}$$

where $\boldsymbol{Q}$ is the power spectral density:

$$\boldsymbol{Q} = \begin{bmatrix} q_{\mathrm{p}} & 0 & 0 \\ 0 & q_{\mathrm{b}} & 0 \\ 0 & 0 & q_{\mathrm{d}} \end{bmatrix} \tag{10}$$

q_{p} is the spectral density value of position,
q_{b} is the spectral density value of clock bias,
q_{d} is the spectral density value of the clock drift.

Then the discrete time linear measurement equation of the system is as follows:

$$\boldsymbol{Z}_k = \boldsymbol{H}_k \boldsymbol{X}_k + \boldsymbol{\xi}_k \tag{11}$$

where
$\boldsymbol{Z}_k$ is the measurement vector of the sensor output,
$\boldsymbol{\xi}_k$ is the white Gaussian observation noise for the sensor with zero mean with obtained covariance matrix $\boldsymbol{R}_k = \boldsymbol{E}\left[\boldsymbol{\xi}_k \ \boldsymbol{\xi}_k^{\mathrm{T}}\right]$,
$\boldsymbol{H}_k$ is the measurement matrix associated with the sensor.

From the model described in Eqs (2), (9), and (11), the KF can be computed as an update stage and a prediction stage [25] as follows.

The update stage

In this stage the KF gain $\boldsymbol{K}_k$ is computed to state estimate measurement update as follows:

$$\hat{\boldsymbol{X}}_k = \hat{\boldsymbol{X}}_{k-1} + \boldsymbol{K}_k \left[\boldsymbol{Z}_k - \boldsymbol{H}_k \hat{\boldsymbol{X}}_{k-1}\right] \tag{12}$$

where the Kalman gain for the data associated to the sensor is expressed as

$$\boldsymbol{K}_k = \boldsymbol{P}_k \boldsymbol{H}_k^{\mathrm{T}} \left(\boldsymbol{H}_k \boldsymbol{P}_k \boldsymbol{H}_k^{\mathrm{T}} + \boldsymbol{R}_k\right)^{-1}$$

and the corrected covariance matrix as follows:

$$\boldsymbol{P}_k = \left[\boldsymbol{I} - \boldsymbol{K}_k \boldsymbol{H}_k\right] \boldsymbol{P}_{k-1} \tag{13}$$

The prediction stage

In this stage, the estimated state $\hat{\boldsymbol{X}}_k$ is corrected whenever a measurement is received. The prediction stage is defined by Eqs (14) and (15):

$$\hat{\boldsymbol{X}}_k = \boldsymbol{\varphi}_{k,k-1} \hat{\boldsymbol{X}}_{k-1} \tag{14}$$

$$\boldsymbol{P}_k = \boldsymbol{\varphi}_{k,k-1} \boldsymbol{P}_{k-1} \boldsymbol{\varphi}_{k,k-1}^{\mathrm{T}} + \boldsymbol{Q}_{k-1} \tag{15}$$

3.2 GPS/INS Integration

In this integration, both the GPS and INS are operated independently, which provides two separate navigation solutions. In order to improve the GPS solution, the position and velocity from GPS are fed to optimal estimator (Kalman filter). On the other hand, the INS solution is also supplied to the integration filter which takes the difference between the two solutions, then, based on the error models it estimates the INS errors. Subsequently, the INS solution is corrected according to the estimated errors in order to provide the integrated navigation solution in the form of position, velocity and attitude. The distinguishing feature of this configuration is a separate filter for the GPS. This integration is an example of cascaded integration because the two filters (the GPS and the integration filters) are used in succession. It is also called a decentralized approach because there is a separate filter used for GPS.

Considering the loosely coupled GPS/INS integration KF, the state vector consists of fifteen states in terms of three position states ($\delta_\varphi\ \delta_\lambda\ \delta_h$), three velocity states ($\delta_{\mathrm{VE}}\ \delta_{\mathrm{VN}}\ \delta_{\mathrm{VU}}$), three attitude states ($\delta_{\mathrm{p}}\ \delta_{\mathrm{r}}\ \delta_{\mathrm{A}}$) in east, north and up directions, three accelerometer biases ($\delta_{fx}\ \delta_{fy}\ \delta_{fz}$), and three gyro drifts respectively ($\delta_{\omega x}\ \delta_{\omega y}\ \delta_{\omega z}$), (the three states for GPS bias in the three directions will be considered later), as follows:

$$\boldsymbol{X} = \left[\delta_\varphi\ \delta_\lambda\ \delta_{\mathrm{h}}\ \delta_{\mathrm{VE}}\ \delta_{\mathrm{VN}}\ \delta_{\mathrm{VU}}\ \delta_{\mathrm{p}}\ \delta_{\mathrm{r}}\ \delta_{\mathrm{A}}\ \delta_{f_x}\ \delta_{f_y}\ \delta_{f_z}\ \delta_{\omega_x}\ \delta_{\omega_y}\ \delta_{\omega_z}\right]^{\mathrm{T}} \tag{16}$$

where

$\left[\delta_{f_x}\ \delta_{f_y}\ \delta_{f_z}\right]$ are three accelerometers constant biases in the body frame, while $\left[\delta_{\omega_x}\ \delta_{\omega_y}\ \delta_{\omega_z}\right]$ are three gyro constant drifts in the body frame.

Position Error for Local Level Frame (LLF)

The position error for Local Level Frame (LLF) in simple form can be obtained as follows:

$$\dot{\boldsymbol{\delta}}_r^l = \boldsymbol{D}^{-1}\boldsymbol{\delta}_r^l$$

applying the orientation of LLF w.r.t earth, where $\boldsymbol{D}^{-1}$transforms the velocity vector from rectangular coordinates into curvilinear coordinates in the Earth-centered earth-fixed (ECEF) frame.

Consequently, the generalized form of the position error will be as follows:

$$\dot{\boldsymbol{\delta}}_r^l = \boldsymbol{\delta}_r^l - \mathrm{skewsymm}\left(\omega_{\mathrm{el}}^l\right) \tag{17}$$

where ω_{el}^l represents the effect of the change of the orientation of local level frame w.r.t the earth and can be represented as follows:

$$\omega_{\mathrm{el}}^l = \begin{bmatrix} -\dot{\varphi} \\ \dot{\lambda}\cos\varphi \\ \dot{\lambda}\sin\varphi \end{bmatrix} = \begin{bmatrix} -\dfrac{v_{\mathrm{n}}}{R_{\mathrm{M}}+h} \\ \dfrac{v_{\mathrm{e}}}{R_{\mathrm{N}}+h} \\ \dfrac{v_{\mathrm{e}}\tan\varphi}{R_{\mathrm{N}}+h} \end{bmatrix} \tag{18}$$

where v_n, v_e, v_u are the velocity components, R_N is the normal radius of curvature for the east-west direction and R_M is the meridian radius of curvature for the north-south direction.

The Velocity Error for Local Level Frame

The velocity error for Local Level Frame (LLF) can be obtained as follows:

$$\dot{V}^l = \boldsymbol{R}_b^l f^b - \left(2\boldsymbol{\Omega}_{\text{ie}}^l + \boldsymbol{\Omega}_{\text{el}}^l\right)V^l + g^l \tag{19}$$

where V is the velocity vector in local level frame, $\boldsymbol{R}_b^l$ is the transformation matrix from the body-frame to the inertial-frame, f^b is the specific force measured by the accelerometers in the body-frame, $\boldsymbol{\Omega}_{\text{ie}}^l$ and $\boldsymbol{\Omega}_{\text{el}}^l$ are the skew-symmetric matrices corresponding to the rotation of the Earth about its spin axis and the change of orientation of the local-level frame with respect to the Earth respectively.

By taking into account the error δ in the measurements, then the velocity error for Local Level Frame (LLF) can be represented as follows:

$$\delta\dot{V}^l = \boldsymbol{R}_b^l\left(f^b + \delta f^b\right) - \left[2\left(\boldsymbol{\Omega}_{\text{ie}}^l + \delta\boldsymbol{\Omega}_{\text{ie}}^l\right) + \left(\boldsymbol{\Omega}_{\text{el}}^l + \delta\boldsymbol{\Omega}_{\text{el}}^l\right)\right]\left(V^l + \delta_v^l\right)\left(g^l + \delta_g^l\right) \tag{20}$$

From Eq. (20), the velocity error for local level frame can be obtained by applying algebraic manipulation to be as follows in Eq. (21).

$$\delta\dot{V}^l = -\boldsymbol{F}^l\boldsymbol{\varepsilon}^l + \boldsymbol{R}_b^l\delta f^b - 2\left(\boldsymbol{\Omega}_{\text{ie}}^l + \boldsymbol{\Omega}_{\text{el}}^l\right)\delta_v^l + V^l\left(2\delta\omega_{\text{ie}}^l + \delta\omega_{\text{el}}^l\right) + \delta_g^l \tag{21}$$

where

$\boldsymbol{F}^l$ is the skew-symmetric matrix corresponding to the specific force,

ω_{ie}^l is angular velocity vector in the LLF obtained from the rotation of earth about its spin axes [ω^e = 15 °/h],

$\boldsymbol{\Omega}_{\text{ie}}^l$ is the skew-symmetric matrix corresponding to ω_{ie}^l,

$\boldsymbol{\Omega}_{\text{el}}^l$ is the skew-symmetric matrix corresponding to ω_{el}^l.

The generalized form for each term of Eq. (21) can be obtained as follows. According to the first term ($F^l\ \varepsilon^l$):

$$\left(F^l\varepsilon^l\right) = \begin{bmatrix} 0 & f_u & f_n \\ f_u & 0 & -f_e \\ -f_n & f_e & 0 \end{bmatrix}\begin{bmatrix} \delta_p \\ \delta_r \\ \delta_a \end{bmatrix} \tag{22}$$

where f_e, f_n, f_u are the body acceleration in east, north and up directions. According to the second term $\left(\boldsymbol{R}_b^l\delta f^b\right)$:

the accelerometer biases δf^b are transformed from the body frame to the LLF using the $\boldsymbol{R}_b^l$ matrix as follows:

$$\left(\boldsymbol{R}_b^l\delta f^b\right) = DCM_{\text{bn}}\begin{bmatrix} \delta_{fx} \\ \delta_{fy} \\ \delta_{fz} \end{bmatrix} = \begin{bmatrix} R_{11} & R_{12} & R_{13} \\ R_{21} & R_{22} & R_{23} \\ R_{31} & R_{32} & R_{33} \end{bmatrix} \tag{23}$$

According to the third term $\left[-2\left(\boldsymbol{\Omega}_{\text{ie}}^l + \boldsymbol{\Omega}_{\text{ie}}^l\right)\delta_{\text{v}}^l\right]$:

$$\left[-2\left(\boldsymbol{\Omega}_{\mathrm{ie}}^{l}+\boldsymbol{\Omega}_{\mathrm{ie}}^{l}\right)\delta_{\mathrm{v}}^{l}\right]=-2\left(\begin{bmatrix}0 & -\omega_{\mathrm{e}}\sin\varphi & \omega_{\mathrm{e}}\cos\varphi\\ \omega_{\mathrm{e}}\sin\varphi & 0 & 0\\ -\omega_{\mathrm{e}}\cos\varphi & 0 & 0\end{bmatrix}+\begin{bmatrix}0 & -\dot{\lambda}\sin\varphi & \dot{\lambda}\cos\varphi\\ \dot{\lambda}\sin\varphi & 0 & \dot{\varphi}\\ -\dot{\lambda}\cos\varphi & -\dot{\varphi} & 0\end{bmatrix}\right)\begin{bmatrix}\delta_{\mathrm{ve}}\\ \delta_{\mathrm{vn}}\\ \delta_{\mathrm{vu}}\end{bmatrix} \quad (24)$$

Rearranging,

$$\left[-2\left(\boldsymbol{\Omega}_{\mathrm{ie}}^{l}+\boldsymbol{\Omega}_{\mathrm{ie}}^{l}\right)\delta_{\mathrm{v}}^{l}\right]=\begin{bmatrix}0 & \left(2\omega_{\mathrm{e}}+\dot{\lambda}\right)\sin\varphi & -\left(2\omega_{\mathrm{e}}+\dot{\lambda}\right)\cos\varphi\\ -\left(2\omega_{\mathrm{e}}+\dot{\lambda}\right)\sin\varphi & 0 & \dot{\varphi}\\ \left(2\omega_{\mathrm{e}}+\dot{\lambda}\right)\cos\varphi & \dot{\varphi} & 0\end{bmatrix}\begin{bmatrix}\delta_{\mathrm{ve}}\\ \delta_{\mathrm{vn}}\\ \delta_{\mathrm{vu}}\end{bmatrix} \quad (25)$$

According to the fourth term $\left(\delta w_{\mathrm{ie}}^{l}+\delta w_{\mathrm{el}}^{l}\right)v^{l}$:

this term can be neglected due to the multiplication of the velocities by the earth rotation rate or by (1/earth radius).

According to the fifth term δ_{g}^{l} :

the term δ_{g}^{l} is the error in normal gravity due primarily to the error in the altitude

$$\delta_{g}^{l}=\begin{bmatrix}-g/r\\ -g/r\\ 2g/\left(r+h\right)\end{bmatrix}\begin{bmatrix}\delta_{\varphi}\\ \delta_{\lambda}\\ \delta_{h}\end{bmatrix} \quad (26)$$

where g represents the normal component of gravity, r is the mean radius of the Earth and h is the height.

The Attitude Error for Local Level Frame

The attitude error for Local Level Frame (LLF) can be obtained as follows:

$$\dot{\boldsymbol{R}}_{b}^{l}=\boldsymbol{R}_{b}^{l}\left[\boldsymbol{\Omega}_{1b}^{l}-\boldsymbol{R}_{l}^{b}\left(\boldsymbol{\Omega}_{\mathrm{ie}}^{l}+\boldsymbol{\Omega}_{\mathrm{el}}^{l}\right)\boldsymbol{R}_{b}^{l}\right] \quad (27)$$

Some terms will be neglected due to the division by earth radius, so the final equation will be as follows

$$\dot{\varepsilon}^{l}=\begin{bmatrix}\dot{\delta}_{\mathrm{p}}\\ \dot{\delta}_{\mathrm{r}}\\ \dot{\delta}_{\mathrm{A}}\end{bmatrix}=-\mathrm{skewsym}\left(\boldsymbol{\Omega}_{\mathrm{ie}}^{l}+\boldsymbol{\Omega}_{\mathrm{el}}^{l}\right)\begin{bmatrix}\delta_{\mathrm{p}}\\ \delta_{\mathrm{r}}\\ \delta_{\mathrm{A}}\end{bmatrix}+DCM_{\mathrm{bn}}\begin{bmatrix}\delta_{\omega_{x}}\\ \delta_{\omega_{y}}\\ \delta_{\omega_{z}}\end{bmatrix} \quad (28)$$

where

$$\mathrm{skewsym}\left(\boldsymbol{\Omega}_{\mathrm{ie}}^{l}+\boldsymbol{\Omega}_{\mathrm{el}}^{l}\right)\begin{bmatrix}\delta_{\mathrm{p}}\\ \delta_{\mathrm{r}}\\ \delta_{\mathrm{A}}\end{bmatrix}=\begin{bmatrix}0 & \left(\omega_{\mathrm{e}}+\lambda_{\mathrm{e}}\right)\sin\varphi & -\left(\omega_{\mathrm{e}}+\lambda_{\mathrm{e}}\right)\cos\varphi\\ -\left(\omega_{\mathrm{e}}+\lambda_{\mathrm{e}}\right)\sin\varphi & 0 & -\varphi\\ \left(\omega_{\mathrm{e}}+\lambda_{\mathrm{e}}\right)\cos\varphi & \dot{\varphi} & 0\end{bmatrix}\begin{bmatrix}\delta_{\mathrm{ve}}\\ \delta_{\mathrm{vn}}\\ \delta_{\mathrm{vu}}\end{bmatrix} \quad (29)$$

The deterministic part of the sensor error (gyro drift and acceleration bias) is computed during the calibration and compensated in the measurements. Also, the non-deterministic is commonly first order Gaussian Markov (GM) and the autoregressive (AR) process.

In general form $\dot{x}=-\beta x+\sqrt{2\beta\delta^{2}\omega}$

where, x is the random process, β is the reciprocal of correlation time, ω is the zero mean Gaussian noise with unit variance, δ^{2} is the variance of white noise.

Accelerometer bias error

$$\begin{bmatrix}\dot{\delta}_{f_x}\\ \dot{\delta}_{f_y}\\ \dot{\delta}_{f_z}\end{bmatrix}=\begin{bmatrix}-\beta_{f_x} & 0 & 0\\ 0 & -\beta_{f_y} & 0\\ 0 & 0 & -\beta_{f_z}\end{bmatrix}\begin{bmatrix}\delta_{f_x}\\ \delta_{f_y}\\ \delta_{f_z}\end{bmatrix}+\begin{bmatrix}\sqrt{2\beta_{f_x}\sigma_{f_x}^2}\\ \sqrt{2\beta_{f_y}\sigma_{f_y}^2}\\ \sqrt{2\beta_{f_z}\sigma_{f_z}^2}\end{bmatrix}w(t) \tag{30}$$

where

$\beta_{f_x},\beta_{f_y},\beta_{f_z}$ are the reciprocals of the correlation times associated with the autocorrelation sequence of $\delta_{f_x},\delta_{f_y},\delta_{f_z}$;

$\sigma_{f_x}^2,\sigma_{f_y}^2,\sigma_{f_z}^2$ are the variances associated with the accelerometer errors;

$w(t)$ is white Gaussian noise.

Gyro bias error

$$\begin{bmatrix}\dot{\delta}_{\omega_x}\\ \dot{\delta}_{\omega_y}\\ \dot{\delta}_{\omega_z}\end{bmatrix}=\begin{bmatrix}-\beta_{w_x} & 0 & 0\\ 0 & -\beta_{w_y} & 0\\ 0 & 0 & -\beta_{w_z}\end{bmatrix}\begin{bmatrix}\delta_{\omega_x}\\ \delta_{\omega_y}\\ \delta_{\omega_z}\end{bmatrix}+\begin{bmatrix}\sqrt{2\beta_{\omega_x}\sigma_{\omega_x}^2}\\ \sqrt{2\beta_{\omega_y}\sigma_{\omega_y}^2}\\ \sqrt{2\beta_{\omega_z}\sigma_{\omega_z}^2}\end{bmatrix}w(t) \tag{31}$$

where

$\beta_{\omega_x},\beta_{\omega_y},\beta_{\omega_z}$ are the reciprocals of the correlation times associated with the autocorrelation sequence of $\delta_{\omega_x},\delta_{\omega_y},\delta_{\omega_z}$;

$\sigma_{\omega_x}^2$, $\sigma_{\omega_y}^2$, $\sigma_{\omega_z}^2$ which are the variances associated with the gyroscope errors.

Based on the above equations and from Eq. (1), the obtained state equation will be as Eq. (32), where $\boldsymbol{F}(t)$ is 15×15 matrix where A_{11} to A_{55} are 3×3 matrices.

$$\begin{bmatrix} \dot{\delta}_{\varphi} \\ \dot{\delta}_{\lambda} \\ \dot{\delta}_{\mathrm{h}} \\ \dot{\delta}_{\mathrm{ve}} \\ \dot{\delta}_{\mathrm{vn}} \\ \dot{\delta}_{\mathrm{vu}} \\ \dot{\delta}_{\mathrm{p}} \\ \dot{\delta}_{\mathrm{r}} \\ \dot{\delta}_{\mathrm{A}} \\ \dot{\delta}_{f_x} \\ \dot{\delta}_{f_y} \\ \dot{\delta}_{f_z} \\ \dot{\delta}_{\omega_x} \\ \dot{\delta}_{\omega_y} \\ \dot{\delta}_{\omega_z} \end{bmatrix} = \begin{bmatrix} A_{11} & A_{12} & A_{13} & A_{14} & A_{15} \\ A_{21} & A_{22} & A_{23} & A_{24} & A_{25} \\ A_{31} & A_{32} & A_{33} & A_{34} & A_{35} \\ A_{41} & A_{42} & A_{43} & A_{44} & A_{45} \\ A_{51} & A_{52} & A_{53} & A_{54} & A_{55} \end{bmatrix} \begin{bmatrix} \delta_{\varphi} \\ \delta_{\lambda} \\ \delta_{\mathrm{h}} \\ \delta_{\mathrm{ve}} \\ \delta_{\mathrm{vn}} \\ \delta_{\mathrm{vu}} \\ \delta_{\mathrm{p}} \\ \delta_{\mathrm{r}} \\ \delta_{\mathrm{A}} \\ \delta_{f_x} \\ \delta_{f_y} \\ \delta_{f_z} \\ \delta_{\omega_x} \\ \delta_{\omega_y} \\ \delta_{\omega_z} \end{bmatrix} + \begin{bmatrix} 0 \\ 0 \\ 0 \\ 0 \\ 0 \\ 0 \\ 0 \\ 0 \\ \sqrt{2\beta_{f_x}\sigma_{f_x}^2} \\ \sqrt{2\beta_{f_y}\sigma_{f_y}^2} \\ \sqrt{2\beta_{f_z}\sigma_{f_z}^2} \\ \sqrt{2\beta_{\omega_x}\sigma_{\omega_x}^2} \\ \sqrt{2\beta_{\omega_y}\sigma_{\omega_y}^2} \\ \sqrt{2\beta_{\omega_z}\sigma_{\omega_z}^2} \end{bmatrix}^{\mathrm{T}} \begin{bmatrix} w_{\varphi} \\ w_{\lambda} \\ w_{\mathrm{h}} \\ w_{\mathrm{ve}} \\ w_{\mathrm{vn}} \\ w_{\mathrm{vu}} \\ w_{\mathrm{p}} \\ w_{\mathrm{r}} \\ w_{\mathrm{A}} \\ w_{f_x} \\ w_{f_y} \\ w_{f_z} \\ w_{\omega_x} \\ w_{\omega_y} \\ w_{\omega_z} \end{bmatrix} \tag{32}$$

Also, the measurement equation according to Eq. (6) will be as follows:

$$\boldsymbol{Z}(t) = [\boldsymbol{H}_1 \ldots . \boldsymbol{H}_{15}] \left[\delta_{\varphi} \delta_{\lambda} \delta_{\mathrm{h}} \delta_{\mathrm{VE}} \delta_{\mathrm{VN}} \delta_{\mathrm{VU}} \delta_{\mathrm{p}} \delta_{\mathrm{r}} \delta_{\mathrm{A}} \delta_{f_x} \delta_{f_y} \delta_{f_z} \delta_{\omega_x} \delta_{\omega_y} \delta_{\omega_z} \right]^{\mathrm{T}} + \boldsymbol{\xi} \tag{33}$$

where $\boldsymbol{H}_1 \ldots \boldsymbol{H}_{15}$ is the measurement matrix associated with the sensor, then the measurement vector can be determined as follows:

$$\begin{aligned} Z(t) = & \\ & [(\varphi_{\mathrm{INS}} - \varphi_{\mathrm{GPS}}) \quad (\lambda_{\mathrm{INS}} - \lambda_{\mathrm{GPS}}) \quad (h_{\mathrm{INS}} - h_{\mathrm{GPS}}) \quad (VE_{\mathrm{INS}} - VE_{\mathrm{GPS}}) \, (VN_{\mathrm{INS}} - VN_{\mathrm{GPS}}) \\ & (VU_{\mathrm{INS}} - VU_{\mathrm{GPS}}) (p_{\mathrm{INS}} - p_{\mathrm{GPS}}) (r_{\mathrm{INS}} - r_{\mathrm{GPS}}) \, (A_{\mathrm{INS}} - A_{\mathrm{GPS}}) \, (fx_{\mathrm{INS}} - fx_{\mathrm{GPS}}) \, (fy_{\mathrm{INS}} - fy_{\mathrm{GPS}}) \\ & (fz_{\mathrm{INS}} - fz_{\mathrm{GPS}}) \, (\omega x_{\mathrm{INS}} - \omega x_{\mathrm{GPS}}) \, (\omega y_{\mathrm{INS}} - \omega y_{\mathrm{GPS}}) (\omega z_{\mathrm{INS}} - \omega z_{\mathrm{GPS}})]^{\mathrm{T}} \end{aligned} \tag{34}$$

Now, considering the three states for GPS bias in the three directions which will be added to the vector states to form eighteen states instead of fifteen in terms of three positions, three velocities, three attitudes in east, north and up directions, three accelerometer biases, three gyro drifts, and three GPS biases in position states as follows:

$$\boldsymbol{X} = \left[\delta_{\varphi} \ \delta_{\lambda} \ \delta_{\mathrm{h}} \ \delta_{\mathrm{ve}} \ \delta_{\mathrm{vn}} \ \delta_{\mathrm{vu}} \ \delta_{\mathrm{p}} \ \delta_{\mathrm{r}} \ \delta_{\mathrm{A}} \ \delta_{f_x} \ \delta_{f_y} \ \delta_{f_z} \ \delta_{\omega_x} \ \delta_{\omega_y} \ \delta_{\omega_z} \ \delta_{\mathrm{GPS}_x} \ \delta_{\mathrm{GPS}_y} \ \delta_{\mathrm{GPS}_z} \right]^{\mathrm{T}} \tag{35}$$

From the above state vector Eq. (35), the dynamic matrix can be obtained by following the same above procedure from Eqs (17)-(32), and consequently the dynamic matrix will be 18×18 matrix including the GPS biases. The dynamic matrix will be 18×18 matrix, where A_{11} to A_{66} are 3×3 matrices.

$$\boldsymbol{F}(t)=\begin{bmatrix} A_{11} & A_{12} & A_{13} & A_{14} & A_{15} & A_{16} \\ A_{21} & A_{22} & A_{23} & A_{24} & A_{25} & A_{26} \\ A_{31} & A_{32} & A_{33} & A_{34} & A_{35} & A_{36} \\ A_{41} & A_{42} & A_{43} & A_{44} & A_{45} & A_{46} \\ A_{51} & A_{52} & A_{53} & A_{54} & A_{55} & A_{56} \\ A_{61} & A_{62} & A_{63} & A_{64} & A_{65} & A_{66} \end{bmatrix} \tag{36}$$

4 Tests and Results

In this section, numerical simulation and field test for the proposed hybrid positioning technique are presented. The performance evaluation in the field test was conducted using a ground vehicle. The vehicle was equipped with a 48 all-in-view tracking Channels BU-353-S4 Waterproof SiRFIV GPS receiver with 1 Hz update rate. In addition, the vehicle was equipped with attitude and heading reference system UM6 ultra-miniature orientation sensor that uses rate gyros, accelerometers, and magnetic sensors to compute sensor orientation 500 times per second.

4.1 Simulation Test

The simulation test is carried out using MATLAB Satellite Navigation toolbox (SatNav). The SatNav was designed for the navigation purpose. The SatNav toolbox simulates satellites and receivers in addition to the standalone positioning algorithms. Also, a real data processing via Receiver Independent Exchange Format version 2 (RINEX2) data file supports the capabilities of the SatNav.

The SatNav toolbox is used to simulate the obtained raw data from GPS that will be used to design KF. Consequently, in order to evaluate the GPS using SatNav, the trajectory that the vehicle will follow should be taken into consideration. Therefore, the trajectory of the obtained navigation solution is shown in Fig. 2a, which shows the division from the true route. Additionally, Fig. 2b shows the estimated path after adding the designed KF to the GPS, where the obtained result is almost identical.

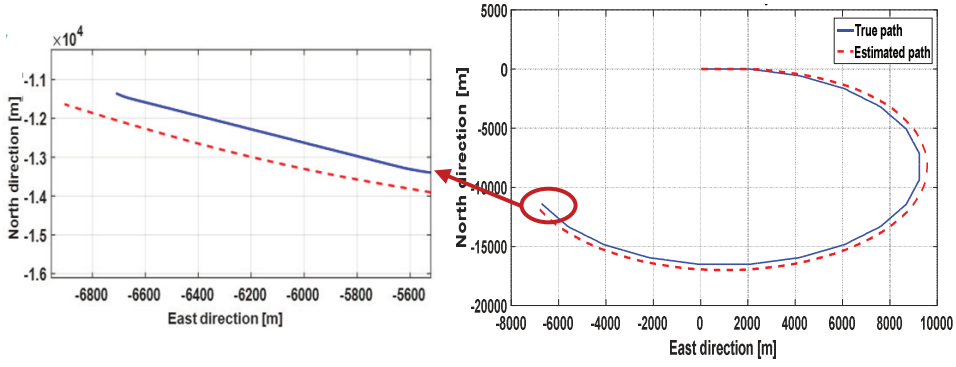

(*a*)

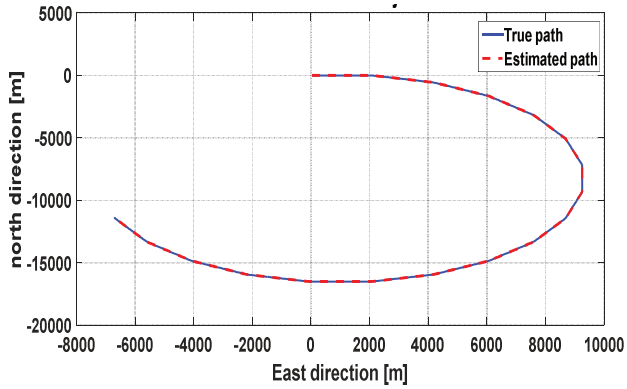

(*b*)

Fig. 2 The true and GPS trajectories without KF, (a) the total difference for GPS with and without KF, (b) The true and GPS trajectories with KF

The average error in position without KF is around 100 m that cause the large division from the true path as shown in Fig. 3a. The error in velocity is shown in Fig. 3b, where the average error in the velocity is around 5 m/s.

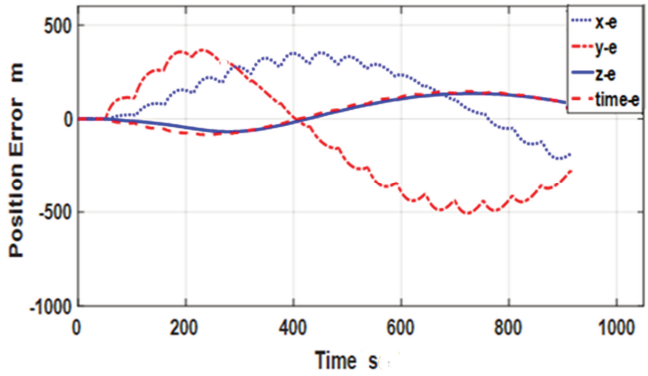

(*a*)

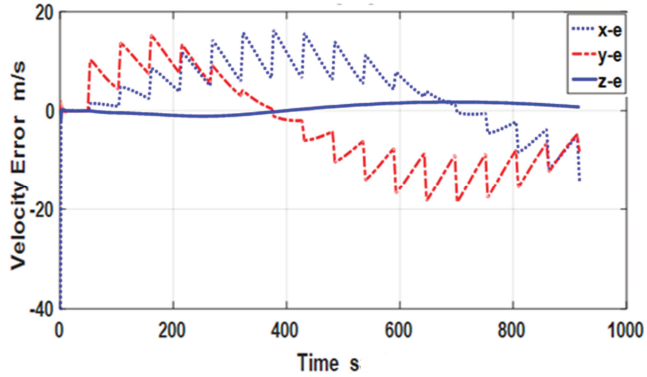

(*b*)

Fig. 3 a) GPS error in position [m]*, b) GPS error in velocity* [m/s]

However, the average error in position for GPS with KF is around 1.5 m as shown in Fig. 4a. The average error in the velocity is around 0.8 m/s as shown in Fig. 4b.

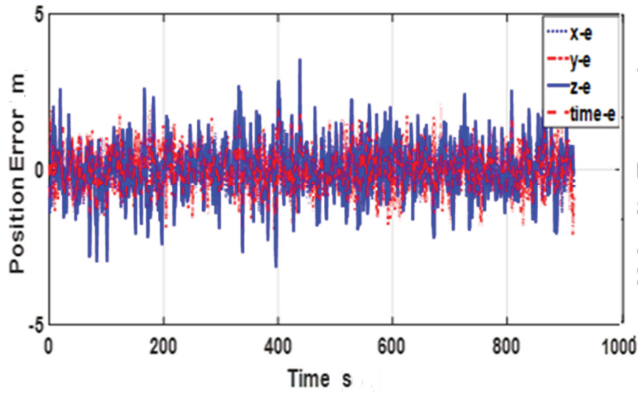

(*a*)

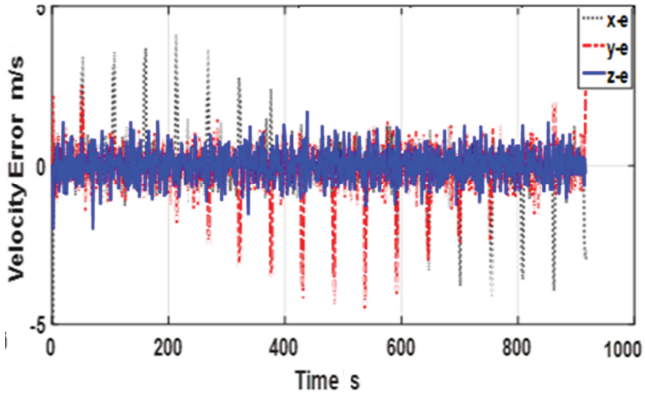

(*b*)

Fig. 4 a) GPS with KF error in position [m]*, b) GPS with KF error in velocity* [m/s]

From the above results it can concluded that the proposed KF for the GPS provides more accurate positioning solution.

4.2 Field Tests

To validate the proposed hybrid positioning framework for GPS/INS integration, a field test was carried out along a pre-described route as shown in Fig. 5a. When the signal of the GPS is available, and the number of the satellite is sufficient, i.e. more than four, the GPS/INS sensor fusion can provide an accurate navigation solution on the first mode. On the other hand, if the number of the available satellites is less than four, the proposed algorithm will switch to the second mode and aiding the INS with GPS raw data will be still possible. The data obtained from the sensors are recorded and applied to the proposed hybrid positioning algorithm to be evaluated.

The obtained results from the field tests are shown in Fig. 5b. The proposed algorithm is validated through two scenarios. The first scenario shows the obtained navigation solution for the field test of the GPS/INS integration in case of the number of satellites is sufficient for the navigation. The second scenario shows the obtained navigation solution of the GPS/INS integration in case of the insufficient number of satellites.

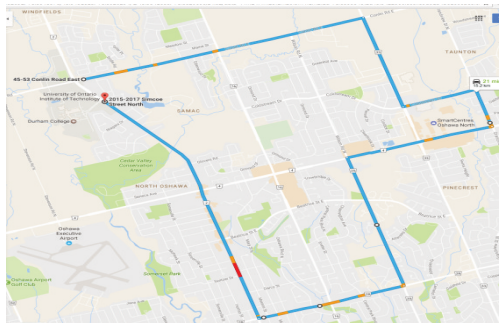

(*a*)

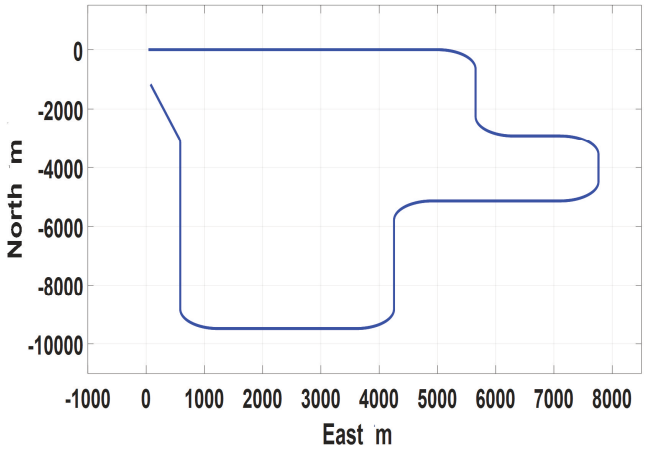

(*b*)

Fig. 5 The proposed route for the field test

The experimental setup for the integrated navigation system is shown in Fig. 6. The system consists of a GPS receiver BU-353-S4, UM6 orientation sensor, power supply, and PC was used as navigation computer. This system allows running the navigation algorithms and logging the navigation sensor data for an offline processing.

a) First Scenario

In this scenario, outdoor experiments were performed to evaluate the navigation system performance in case of a sufficient number of satellites (more than 4 satellites). In addition, the obtained outputs resulting from the developed fifteen and eighteen states KF will be compared.

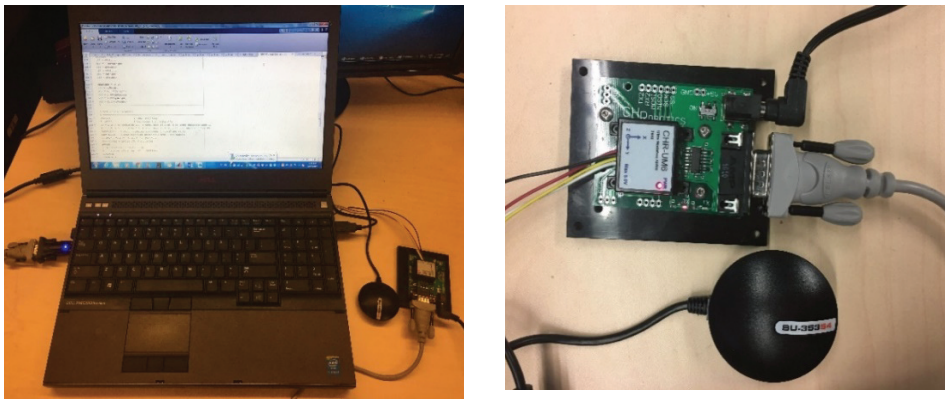

Fig. 6 Experimental integrated navigation system.

KF with 15 states

The results obtained by using fifteen KF states are analyzed in terms of the horizontal position error as shown in Fig. 7. The average value of the error is around 2 m within 14 min. The error in position is shown in Fig. 8, where the error for aided latitude and longitude is almost zero compared with the unaided case. The overall accumulation error in horizontal position is shown in Fig. 9, where the error reaches 400 m within 14 min.

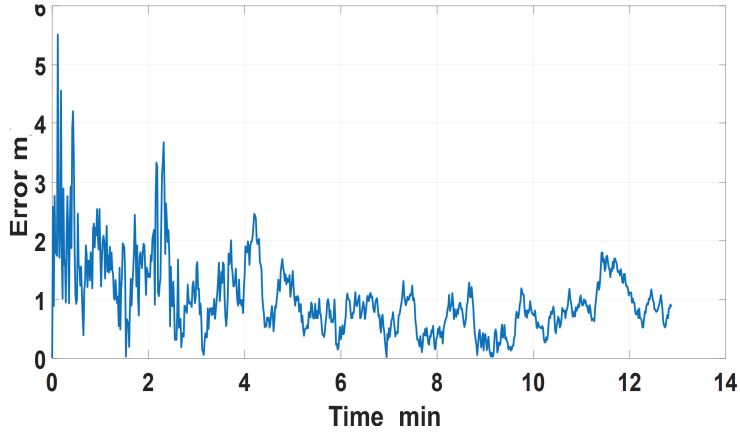

Fig. 7 Horizontal position error for fifteen state KF

Furthermore, the covariance analysis of the position RMS is shown in Fig. 10, which shows that the RMS error for x and y position decreased and became around 1 m. Consequently, Fig. 11 shows the velocity covariance in *x* and *y* decreased to around 0.1 m/s.

The obtained results of the velocity errors in the north, east and up frame are shown in Fig. 12. They show the difference between the aided and unaided INS outputs. Consequently, it can be noticed that the velocity error was accumulated for the unaided INS scenario. The errors in the attitude angles for both aided and unaided are shown in Fig. 13, where all are zeros.

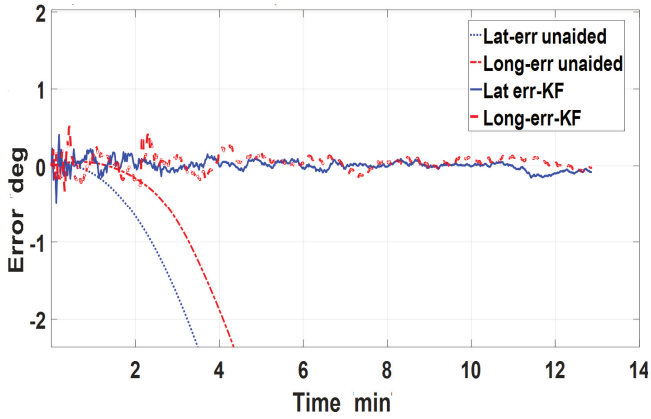

Fig. 8 Lat, Long error aided and unaided KF

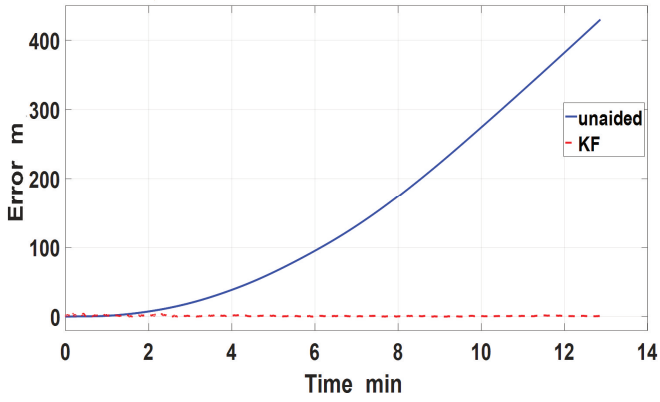

Fig. 9 Horizontal position error

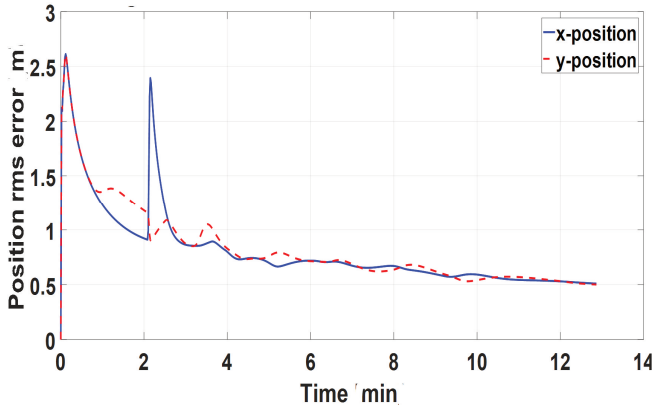

Fig. 10 Covariance analysis of the position RMS error

DOI 10.3849/aimt.01498

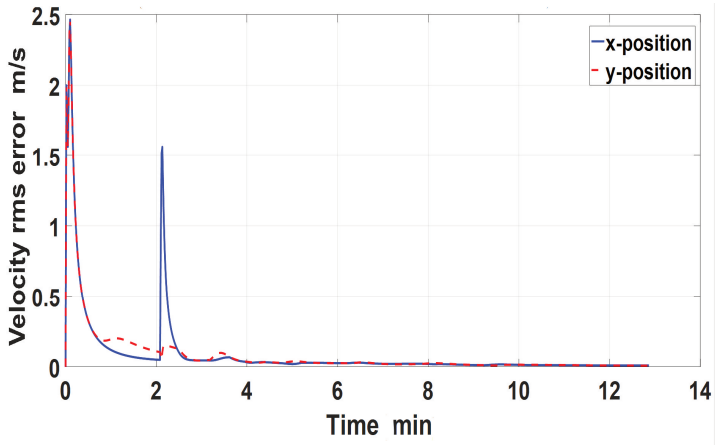

Fig. 11 Covariance analysis of the velocity

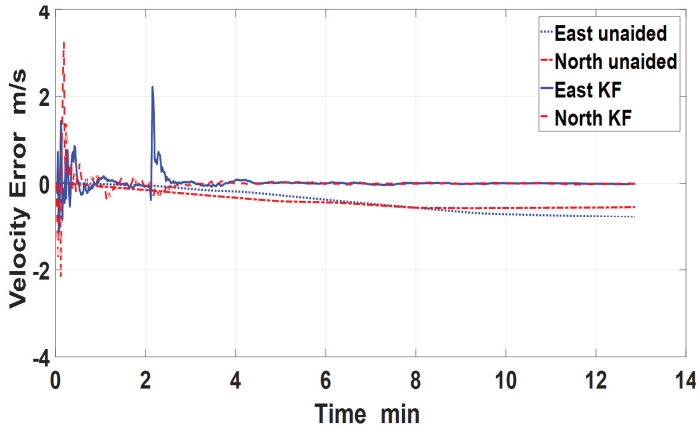

Fig. 12 The velocity error in fifteen state KF

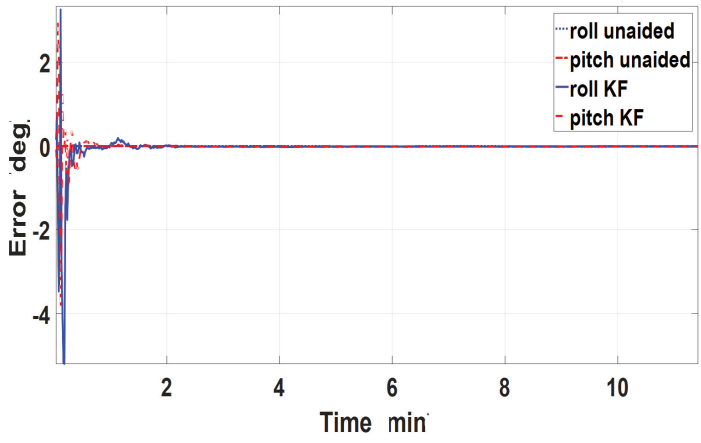

Fig. 13 Attitude angles error

KF with 18 states

The performance evaluation in terms of the horizontal position error for eighteen and fifteen KF states is analyzed as shown in Fig. 14. The obtained results clarify that the average value of the horizontal error using the eighteen KF is around 0.9 m within 14 min which provides better accuracy compared with the fifteen KF that provides average error around 1.8 m within 14 min. Consequently, the velocity errors in north, east and up frame are shown in Fig. 15, which is showing the difference between the aided and unaided INS. Notice that the velocity error is accumulated in case of unaided data. Also, the error in position is shown in Fig. 16. Consequently, it can be noticed that the error using the aided latitude and longitude are almost zero compared with the error in case of unaided latitude and longitude.

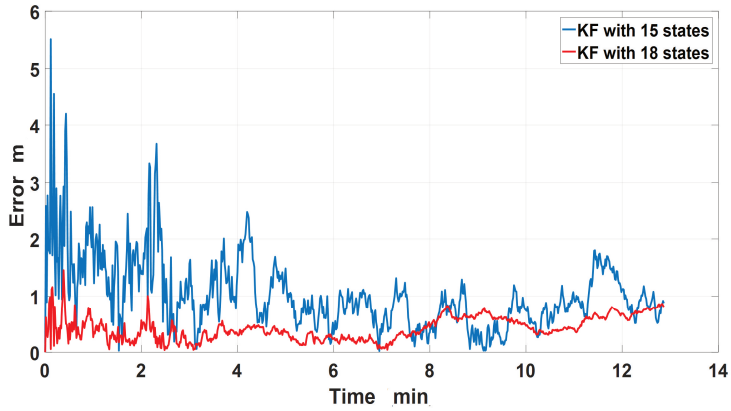

Fig. 14 Horizontal position error for fifteen and eighteen KF states

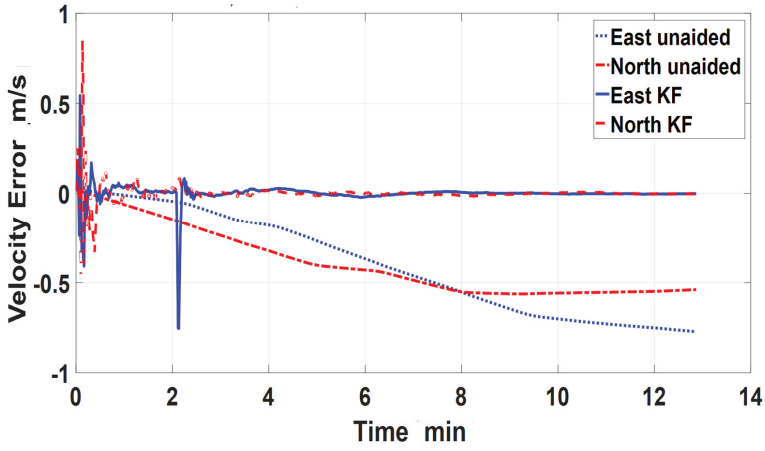

Fig. 15 The velocity error in eighteen KF states

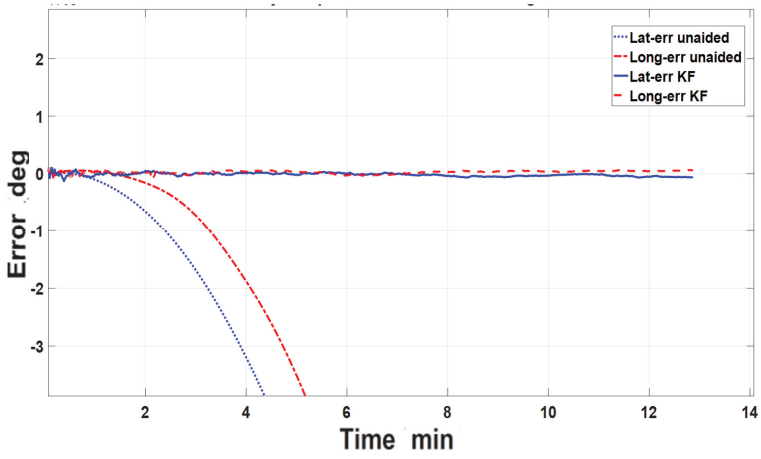

Fig. 16 Lat, Long error aided and unaided KF

Based on the obtained results, the navigation solution of the proposed eighteen states algorithm provides better accuracy than the fifteen KF states in terms of the RMS and maximum values of the position error. Therefore, the eighteen states algorithm will be used to perform as a second mode if the visible number of satellites is less than four.

b) Second Scenario

In this scenario, field experiments were performed to evaluate the navigation system performance in case of an insufficient number of satellites. In this scenario, the simulated number of the available satellites that received by the GPS receiver will be decreased with time, and the number of satellites degradation over time is shown in Fig. 17. Consequently, it can be noticed that the GPS started to receive the data from eight satellites, i.e. the number of satellites is sufficient in the first step. Subsequently, after five minutes the number of satellites decreased to four satellites, then after six minutes it was three satellites for six minutes. Accordingly, the estimated error in horizontal position is shown in Fig. 18, which shows the effect of satellites degradation on the horizontal error, where the average value of the error is around 2 m within 14 min. It reflects an accurate performance with satellites degradation. The velocity errors in north, east and up frame are shown in Fig. 19, which shows the difference between the aided and unaided INS. Thus, the velocity error is accumulated in case of unaided INS. In addition, the errors in the attitude angles for both aided and aided are shown in Fig. 20, where all errors converge to zeros.

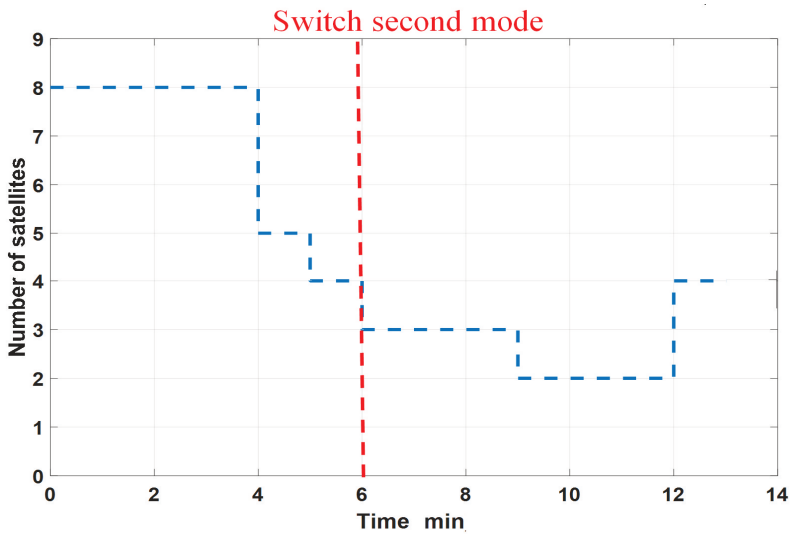

Fig. 17 GPS satellites degradation over the time

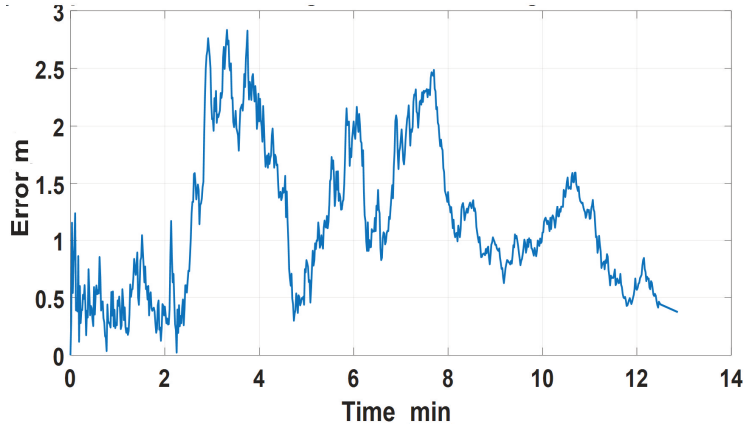

Fig. 18 Horizontal position error for KF state

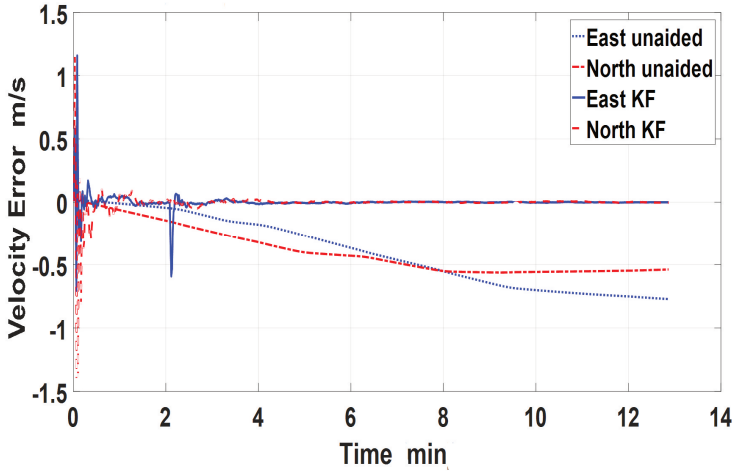

Fig. 19 Velocity error

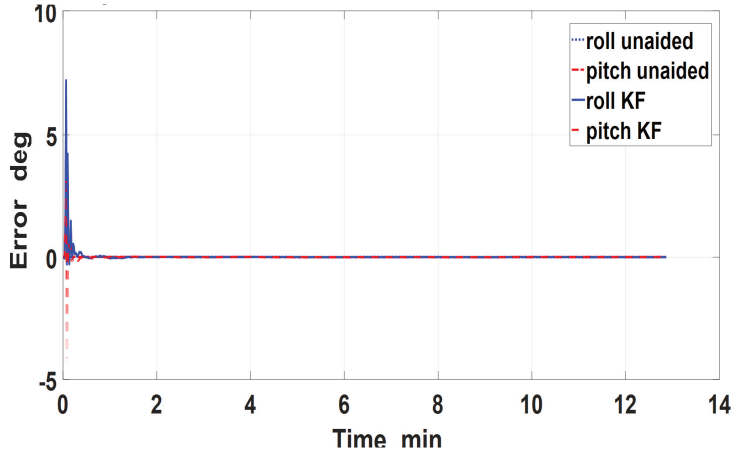

Fig. 20 Attitude angles error

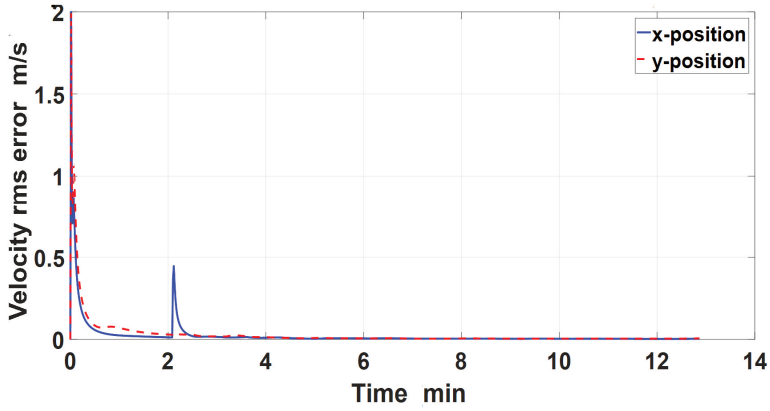

Fig. 21 Covariance analysis of the velocity RMS error

Furthermore, Fig. 21 shows the velocity covariance analysis, in which x and y decreased to be around 0.05 m/s. Consequently, the covariance analysis of the RMS position is shown in Fig. 22, which shows that RMS for x and y positions decreased to around 1.5 m.

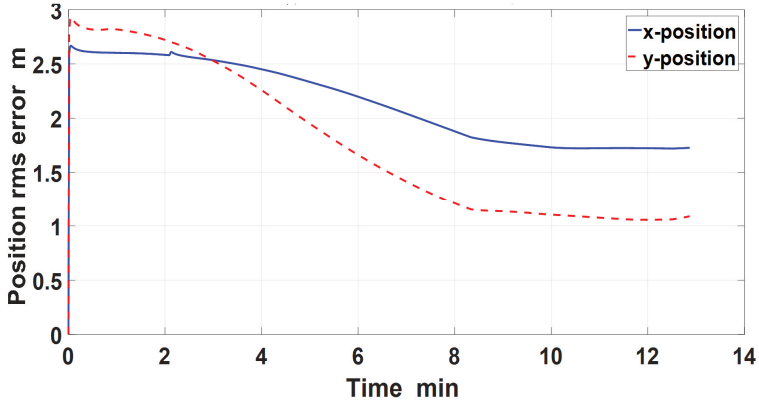

Fig. 22 Covariance analysis of the position RMS error

The error in position is illustrated in Fig. 23, which shows that the errors in aided lateral and longitudinal positions are almost zero compared with the unaided one. This scenario clearly shows that the proposed method can provide more accurate positioning solution, even if the number of satellites falls below the minimum.

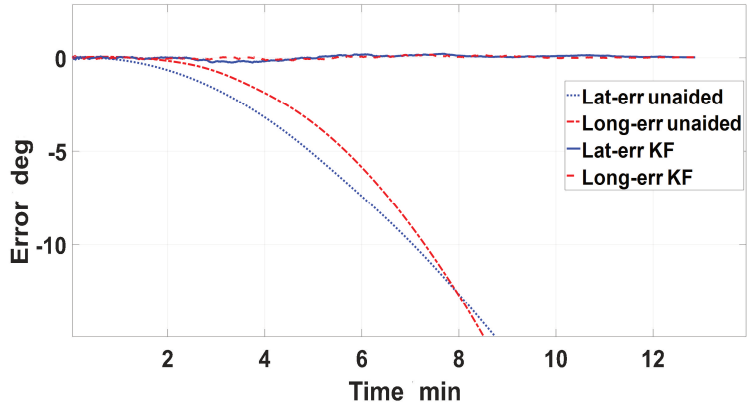

Fig. 23 Lat, Long error aided and unaided KF

5 Conclusion

In the research described in this paper, a hybrid framework for positioning technique based on the integration of GPS/INS has been successfully developed to achieve a robust positioning performance for autonomous combat vehicles. The proposed algorithm has the capability to adapt itself to solving the problem when the number of visible satellites is less than four by switching between the introduced two modes. In addition, the proposed algorithm is able to fuse the obtained data from low-cost sensors such as the GPS and the INS. For this purpose, two Kalman filters have been developed; the first one to improve the GPS information, and the second one to en-

hance the INS position, velocity and attitude with the aid of GPS position and velocity. In addition, the introduced algorithm has the capability to enhance the navigation solution obtained from the low-cost sensors compared with the tactical grade sensors. Based on the covariance analysis of the RMS position using fifteen KF states, RMS error for x and y positions decreased and became around 1 m, while the velocity covariance in x and y decreased to around 0.1 m/s. Moreover, from the velocity errors in the north, east and up frame it can be noticed that the velocity error was accumulated for the unaided INS case. In addition, the errors in the attitude angles for both aided and unaided positions are all zeros. However, the average value of the horizontal error using the eighteen KFs is around 0.9 m within 14 min which provides better accuracy compared with the fifteen KFs which provides an average error around 1.8 m within 14 min. The errors in both aided latitude and longitude cases are almost zero compared with the unaided one. In addition, the execution time using the loosely coupled integration is lower than the execution time of the tightly coupled integration. Accordingly, this work was developed in order to obtain this benefit by using loosely coupled integration combined with the tightly coupled integration and to reduce the execution time of the navigation solution. A simulation and field tests were conducted to evaluate the performance of the developed hybrid algorithm. The simulation was performed using a SATNAV navigation toolbox in MATLAB. The field test was carried out by collecting the navigation data from the sensors mounted on the ground vehicle. The simulation and experimental results show that the proposed framework has the capability to improve the positioning accuracy by switching between the two modes, even if the available number of visible satellites falls below the minimum. Furthermore, in the future work the developed algorithm will be implemented on Cortex m4 Board for real time testing and investigation.

References

[1] BROWN, M., J. FUNKE, S. ERLIEN and J.C. GERDES. Safe Driving Envelopes for Path Tracking in Autonomous Vehicles. *Control Engineering Practice*, 2017, **61**, pp. 307-316. ISSN 0967-0661.

[2] MOHAMED, A., M. EL-GINDY, J. REN and H. LANG. Optimal Collision-Free Path Planning for an Autonomous Multi-Wheeled Combat Vehicle. In: *ASME International Design Engineering Technical Conferences and Computers and Information in Engineering Conference*. Cleveland: ASME, 2017, V003T01A002. DOI 10.1115/DETC2017-67025.

[3] JARVIS, R. An All-Terrain Intelligent Autonomous Vehicle with Sensor-Fusion-Based Navigation Capabilities. *Control Engineering Practice*, 1996, **4**(4), pp. 481-486. DOI 10.1016/0967-0661(96)00029-9.

[4] MOHAMED A, J. REN, H. LANG and M. EL-GINDY. Optimal Collision Free Path Planning for an Autonomous Articulated Vehicle with Two Trailers. In: *IEEE International Conference on Industrial Technology (ICIT)*. Toronto: IEEE, 2017, pp. 860-865. DOI 10.1109/ICIT.2017.7915472.

[5] MOHAMED, A., A.N. OUDA, J. REN and M. EL-GINDY. Processor-in-the-Loop Co-Simulations and Control System Design for a Scaled Autonomous Multi-Wheeled Combat Vehicle. *International Journal of Automation and Control,* 2020, **14**(2), pp. 138-160. DOI 10.1504/IJAAC.2020.105516.

[6] WU, Z., M. YAO, H. MA and W. JIA. Improving Accuracy of the Vehicle Attitude Estimation for Low-Cost INS/GPS Integration Aided by the GPS-Measured Course Angle. *IEEE Transactions on Intelligent Transportation Systems*, 2013, **14**(2), pp. 553-564. DOI 10.1109/TITS.2012.2224343.

[7] SANTOS, M.C.P., L.V. SANTANA, M. SARCINELLI-FILHO and R. DCA-RELLIE. Indoor Low-Cost Localization System for Controlling Aerial Robots. *Control Engineering Practice*, 2017, **61**, pp. 93-111. DOI 10.1016/j.conengprac.2017.01.011.

[8] SHAGHAGHIAN, A. and P. KARIMAGHAEE. Improving GPS/INS Integration Using FIKF-Filtered Innovation Kalman Filter. *Asian Journal of Control*, 2019, **21**(4), pp. 1671-1680. DOI 10.1002/asjc.1931.

[9] WERRIES, A. and J.M. DOLAN. Adaptive Kalman Filtering Methods for Low-Cost GPS/INS Localization for Autonomous Vehicles [online]. Pittsburgh: Carnegie-Mellon University, 2016 [viewed 2019-11-12]. DOI 10.1184/R1/6551687.v1. Available at: https://rosap.ntl.bts.gov/view/dot/36294

[10] LIU, Y., X. FAN, C. LV, J. WU, L. LI and D. DING. An Innovative Information Fusion Method with Adaptive Kalman Filter for Integrated INS/GPS Navigation of Autonomous Vehicles. *Mechanical Systems and Signal Processing,* 2018, **10**, pp. 605-616. DOI 10.1016/j.ymssp.2017.07.051.

[11] SHEN, C., Y. ZHANG, J. TANG, H. CAO and J. LIU. Dual-Optimization for a MEMS-INS/GPS System during GPS Outages Based on the Cubature Kalman Filter and Neural Networks. *Mechanical Systems and Signal Processing,* 2019, **133**, pp. 106-222. DOI 10.1016/j.ymssp.2019.07.003.

[12] MOORE, T. and D.W. STOUCH. A Generalized Extended Kalman Filter Implementation for the Robot Operating System. In: MENEGATTI, E., N. MICHAEL, K. BERNS, H. YAMAGUCHI, eds. *Intelligent Autonomous Systems 13*. Cham: Springer, 2015, pp. 335-348. ISBN 978-3-319-08338-4.

[13] LI, D., X. JIA and J. ZHAO. A Novel Hybrid Fusion Algorithm for Low-Cost GPS/INS Integrated Navigation System during GPS Outages. *IEEE Access,* 2020, **8**, pp. 53984-53996. DOI 10.1109/ACCESS.2020.2981015.

[14] KALMAN, R.E. New Approach to Linear Filtering and Prediction Problems. *Journal of Fluids Engineering*, 1960, **80**(1), pp. 35-45. DOI 10.1115/1.3662552.

[15] HAO, Y., A. XU, X. SUI and Y.WANG. A Modified Extended Kalman Filter for a Two-Antenna GPS/INS Vehicular Navigation System. *Sensors,* 2018, **18**(11), 3809. DOI 10.3390/s18113809.

[16] SASANI, S., J. ASGARI and A.R. AMIRI-SIMKOOEI. Improving MEMS-IMU/GPS Integrated Systems for Land Vehicle Navigation Applications. *GPS solutions,* 2016, **20**, pp. 89-100. DOI 10.1007/s10291-015-0471-3.

[17] CARON, F., E. DUFLOS, D. POMORSKI and P. VANHEEGHE. GPS/IMU Data Fusion Using Multisensor Kalman Filtering: Introduction of Contextual Aspects. *Information Fusion,* 2006, **7**, pp. 221-230. DOI 10.1016/j.inffus.2004.07.002.

[18] LEE, Y., J. YOON, H. YANG, C. KIM and D. LEE. Camera-GPS-IMU Sensor Fusion for Autonomous Flying. In*: 2016 Eighth International Conference on*

Ubiquitous and Future Networks (ICUFN). Vienna: IEEE, 2016, pp. 85-88. DOI 10.1109/ICUFN.2016.7536988.

[19] WANG, S., S. DENG and G. YIN. An Accurate GPS-IMU/DR Data Fusion Method for Driverless Car Based on a Set of Predictive Models and Grid Constraints. *Sensors*. 2016, **16**(3), 280. DOI 10.3390/s16030280.

[20] BOSTANCI, E., B. BOSTANCI, N. KANWAL and A.F. CLARK. Sensor Fusion of Camera, GPS and IMU Using Fuzzy Adaptive Multiple Motion Models. *Soft Computing*, 2018, **22**, pp. 2619-2632. DOI 10.1007/s00500-017-2516-8.

[21] TIAN, J., Y. LIU, Y. WU, Y. LU and Z. HE. GPS/INS Fusion Algorithm Based on Variational Bayesian Adaptive Kalman Filter. *International Core Journal of Engineering*, 2021, **7**(2), pp. 26-32. DOI 10.6919/ICJE.202102_7(2).0005.

[22] SCHERZINGER, B.M. Precise Robust Positioning with Inertial/GPS RTK. *Navigation*, **53**(2), pp. 73-83. DOI 10.1002/j.2161-4296.2000.tb00374.x.

[23] NOURELDIN, A., T.B. KARAMAT and J. GEORGY. *Fundamentals of Inertial Navigation, Satellite-Based Positioning and Their Integration*. Berlin: Springer, 2013. ISBN 978-3-642-44790-7.

[24] FARRELL, J.A., T.D. GIVARGIS and M.J. BARTH. Real-Time Differential Carrier Phase GPS-Aided INS. *IEEE Transactions on Control Systems Technology,* 2000, **8**(4), pp. 709-721. DOI 10.1109/87.852915.

[25] BAR-SHALOM, Y., X.-R. LI and T. KIRUBARAJAN. *Estimation with Applications to Tracking and Navigation: Theory Algorithms and Software*. Hoboken: Wiley, 2004. ISBN 978-0-471-41655-5.